Supporting Information

Electrodeposited Ni_3Fe alloy on carbon cloth for efficient oxygen evolution

Chenyu Shi[a], Junjun Zhang[a*], Jie Yuan[c], Yizhu Lei[c*], Pengfei Zhang[a,b*]

[a.] State Key Laboratory of High-efficiency Utilization of Coal and Green Chemical Engineering, College of Chemistry & Chemical Engineering, Ningxia University, Yinchuan, 750021, Ningxia. China. E-mail: zhangjj089@nxu.edu.cn pfzhang@nxu.edu.cn
[b.] School of Chemistry and Chemical Engineering, Shanghai Jiao Tong University, Shanghai, 200240, China. E-mail: chemistryzpf@sjtu.edu.cn
[c.] School of Chemistry and Materials Engineering, Liupanshui Normal University, Liupanshui, 553004, Guizhou. China E-mail: yzleiabc@lpssy.edu.cn

1. Experimental Section:

2. Supplementary Figures:

3. Supplementary Table

4. References

1 Experimental Section

1.1 Materials

Anhydrous iron chloride ($FeCl_3$), anhydrous cobalt chloride ($CoCl_2$), anhydrous manganese chloride ($MnCl_2$), nickel chloride hexahydrate ($NiCl_2·6H_2O$), sodium chloride (NaCl), and Nafion (5 wt%) were purchased from Aladdin Group Chemical Reagent Co., Ltd. Milli-Q ultrapure water was used throughout all experiments. All chemicals were of analytical grade and used as received without further purification.

1.2 Synthesis of NiM/CC

Synthesis of Ni_3Fe/CC

First, 15 mmol of nickel chloride hexahydrate ($NiCl_2·6H_2O$), 5 mmol of anhydrous iron chloride ($FeCl_3$), and 10 mmol of sodium chloride (NaCl) were dissolved in 100 mL of deionized water. The mixture was continuously stirred for 30 minutes to achieve homogeneous mixing, forming the precursor electrolyte.

A standard three-electrode system was used for electrodeposition: the pretreated carbon cloth (CC) served as the working electrode, a 1 cm × 1 cm platinum sheet serving as the counter electrode, and an Ag/AgCl electrode as the reference electrode. Electrodeposition was conducted at room temperature with a constant current density of −100 $mA·cm^{-2}$ for 200 s, 400 s, and 600 s, and the as-prepared samples were denoted as Ni_3Fe 200s, Ni_3Fe 400s, and Ni_3Fe 600s, respectively. After deposition, the working electrode was immediately removed, rinsed with deionized water for 5 seconds, and then dried in an oven at 60°C for 6 hours. Finally, the Ni_3Fe/CC electrocatalysts were successfully obtained.

Synthesis of Ni_3Mn/CC

Anhydrous ferric chloride ($FeCl_3$) was replaced with anhydrous manganese chloride ($MnCl_2$), while all other synthetic parameters and procedures remained identical to those for Ni_3Fe/CC.

Synthesis of Ni_3Co/CC

Anhydrous ferric chloride ($FeCl_3$) was replaced with anhydrous cobalt chloride ($CoCl_2$), while all other synthetic parameters and procedures remained identical to those for Ni_3Fe/CC.

synthesis of Ni/CC

The synthetic protocol was identical to that of Ni_3Fe/CC except for the removal of $FeCl_3$. Specifically, 15 mmol of $NiCl_2 \cdot 6H_2O$ and 10 mmol of NaCl were dissolved in 100 mL of deionized water, followed by the same stirring, electrodeposition, rinsing, and drying processes.

1.3 Synthesis of RuO_2

5 mg of RuO_2 powder was dispersed in a mixed solution containing 500 μL deionized water, 480 μL ethanol and 20 μL Nafion solution. The mixture was subjected to ultrasonic treatment for 30 min to form a homogeneous catalyst ink. The obtained ink was uniformly coated onto the pre-treated carbon cloth (CC), and naturally dried at ambient temperature prior to subsequent storage.

1.4 Material characterizations

The X-ray diffraction (XRD) patterns were recorded on a Bruker D8 Advance X-ray diffractometer with Cu-Kα radiation (λ = 1.5418 Å) at a scan rate of 6° min^{-1}. The SEM measurements were performed on a field-emission scanning electron microscope (FESEM, JSM-7610F, 10 kV). The TEM and HRTEM measurements were taken with a JEOL JEM-F200 microscope. The samples were prepared by dropping an ethanol dispersion of the samples onto carbon-coated copper TEM grids with pipettes and dried under ambient conditions. The X-ray photoelectron spectroscopy (XPS) measurements were conducted on a Kratos Axis Ultra DLD spectrometer. Raman measurements were performed using a JY HR800 Raman spectrometer.

1.5 Electrochemical characterizations

Electrochemical performance tests were performed at room temperature using an electrochemical workstation (DH7000C, Donghua, China). A three-electrode system was used, where Ni_3Fe/CC served as the working electrode, a graphite rod serving as the counter electrode, and a standard Hg/HgO electrode as the reference electrode. A 1.0 M KOH solution was employed as the electrolyte.

All recorded potentials were converted to the reversible hydrogen electrode (RHE) scale according to the equation: $E_{RHE} = E_{Hg/HgO} + 0.059\ pH + 0.098\ V$. All polarization curves were measured at a scan rate of 10 mV s^{-1} and corrected with iR compensation. The solution resistance (Rs) was determined from the high-frequency intercept of Nyquist plots. The iR-corrected potential was calculated as $E_{corrected} = E_{measured} - i*R_s$,

where $E_{corrected}$ and $E_{measured}$ are the iR-compensated and experimentally measured potentials, respectively, and Rs is the uncompensated solution resistance. Before electrochemical testing, 20 cyclic voltammetry (CV) cycles were conducted between 0.5 and 1.2 V vs. Hg/HgO at 10 mV s^{-1} to stabilize the electrode surface. Linear sweep voltammetry (LSV) was measured over the range of 0-1.2 V vs. Hg/HgO. Electrochemical impedance spectroscopy (EIS) was carried out over a frequency range from 100 kHz to 0.1 Hz, and operando EIS tests were performed at various applied potentials in the range of 0.50–0.80 V vs. Hg/HgO.

The overpotential (η) was calculated by $\eta = E_{RHE} - 1.23$. Tafel plots were derived from the iR-corrected polarization curves by plotting overpotential versus logarithmic current density, and the Tafel slope was obtained by fitting the linear region according to $\eta = b \log(j) + a$. Long-term durability was evaluated by chronopotentiometric measurements under constant current density. All these electrochemical measurements were carried out at ambient temperature.

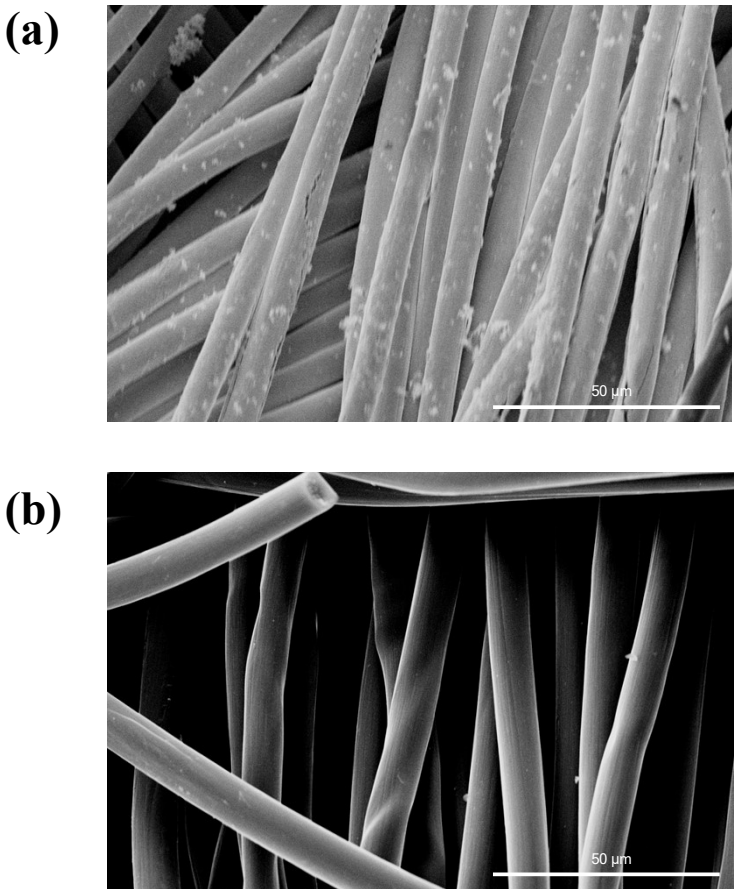

Fig S1. SEM images of the (a) Ni_3Fe/CC sample and (b) CC substrate.

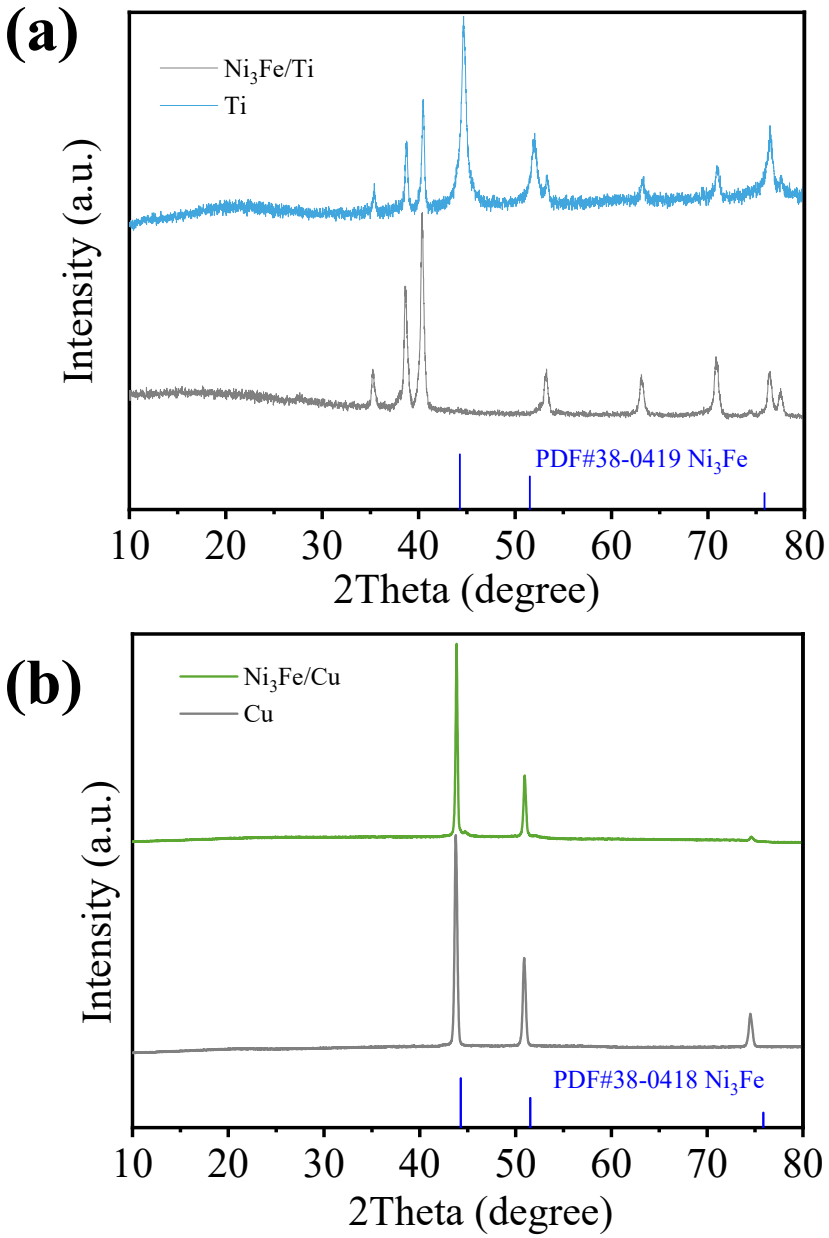

Fig S2. XRD patterns of Ni_3Fe sample on (a) Ti and (b) Cu substrates.

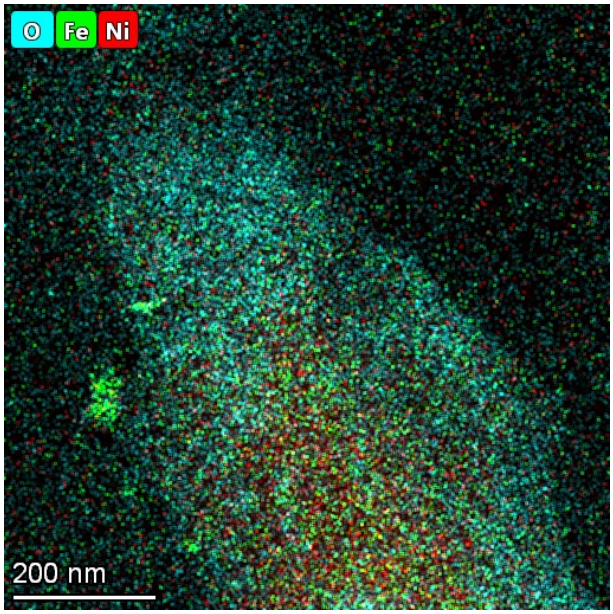

Fig S3. Elemental mapping image of Ni_3Fe/CC.

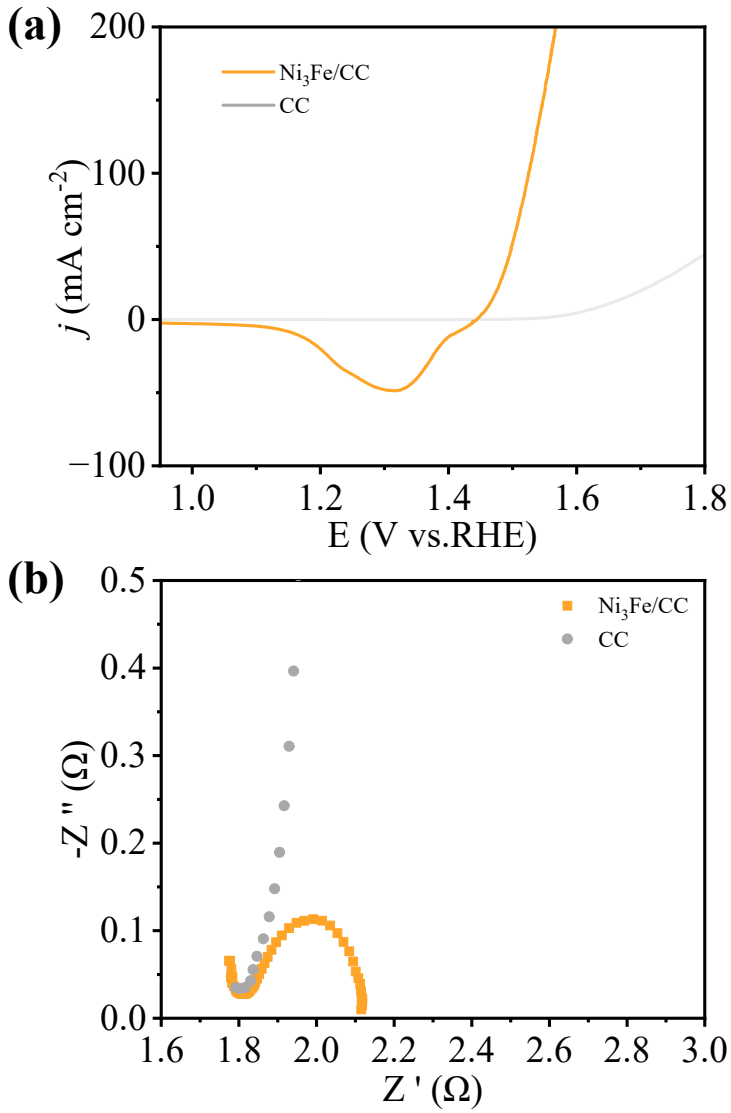

Fig S4. (a) LSV curves and (b) EIS of Ni_3Fe sample on CC substrate.

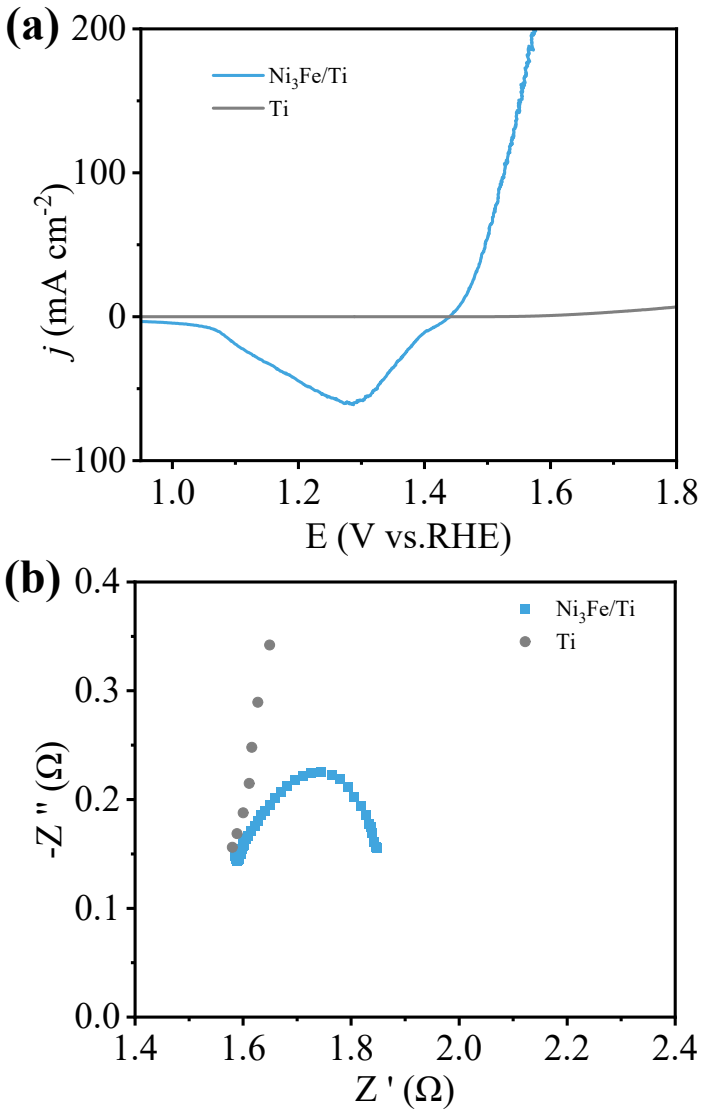

Fig S5. (a) LSV curves and (b) EIS of Ni_3Fe sample on Ti substrate.

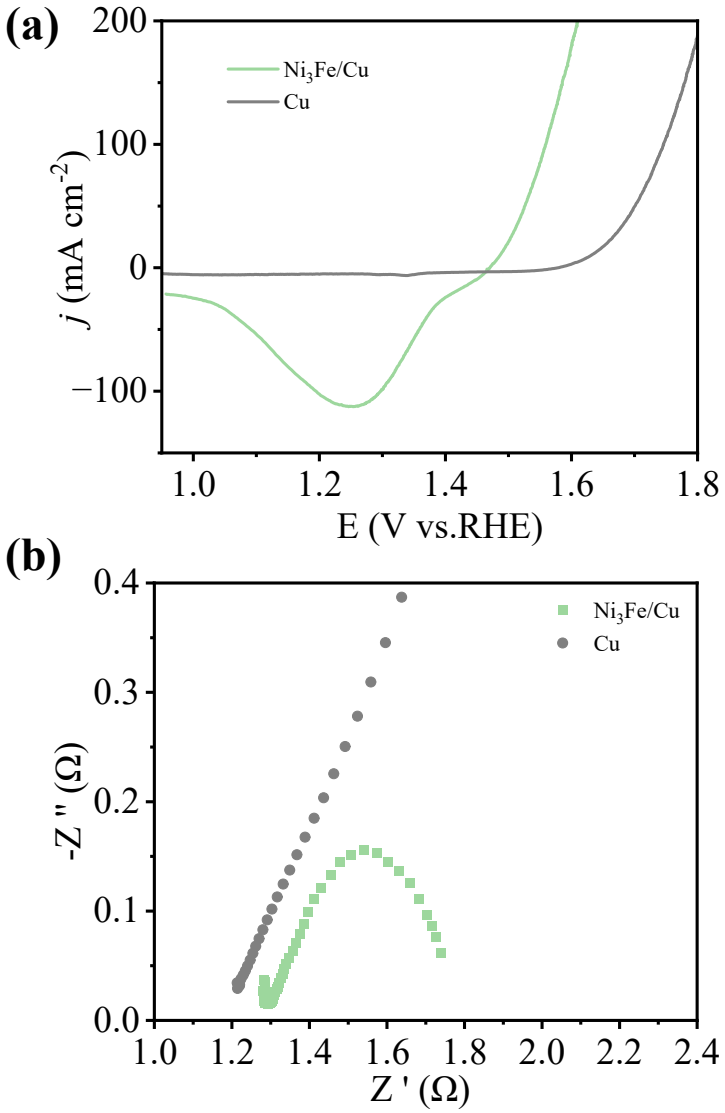

Fig S6. (a) LSV curves and (b) EIS of Ni_3Fe sample on Cu substrate.

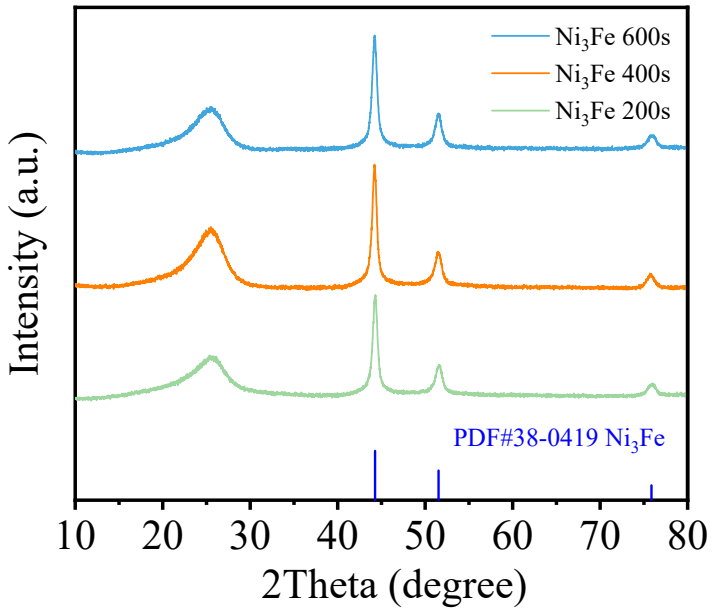

Fig S7. XRD patterns of Ni_3Fe/CC samples prepared with different electrodeposition times.

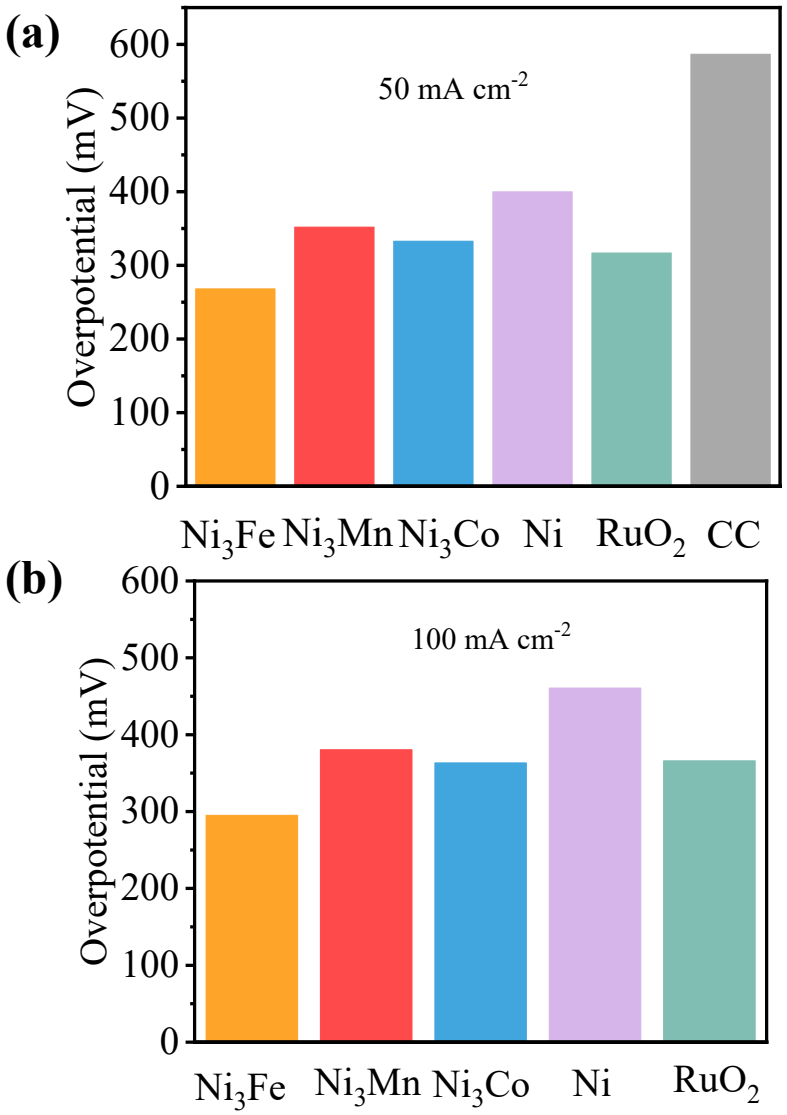

Fig S8. Overpotentials of Ni_3Fe/CC, Ni_3Mn/CC, Ni_3Co/CC, Ni/CC, CC and RuO_2 electrodes at current densities of (a) 50 mA·cm^{-2} and (b) 100 mA·cm^{-2}

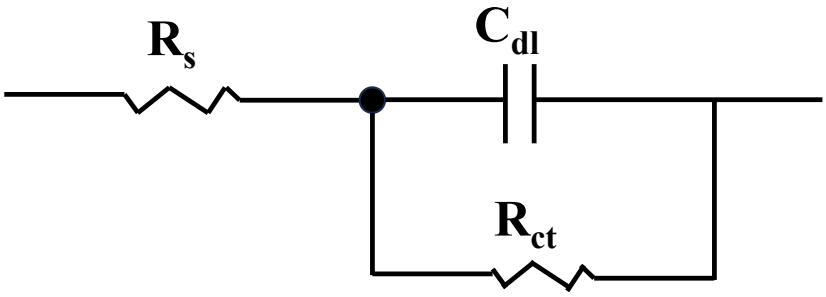

Fig S9. Schematic of the equivalent circuit used for electrochemical impedance spectroscopy.

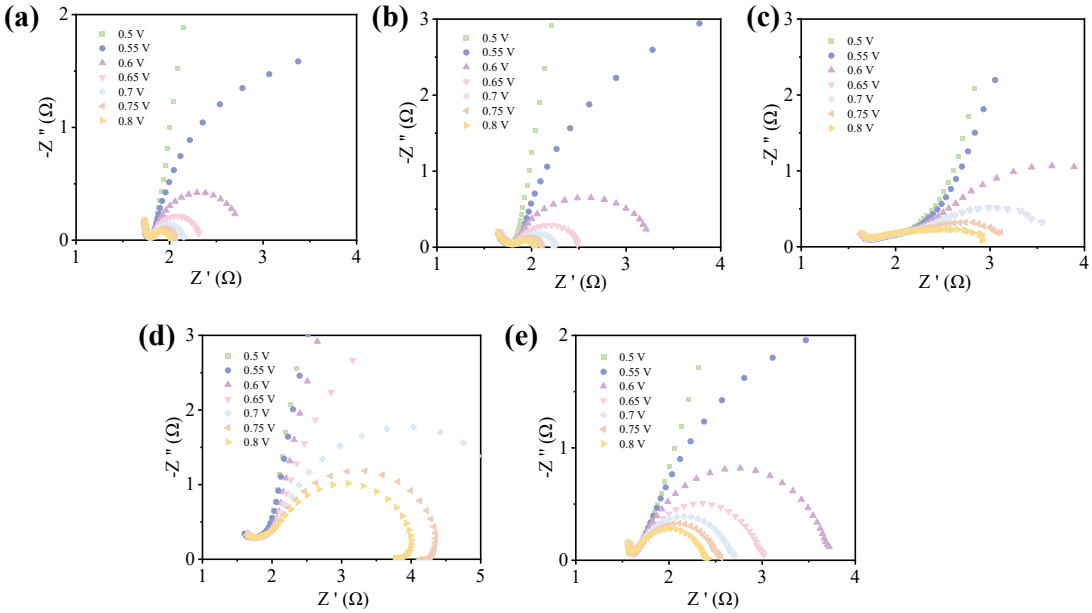

Fig S10. The Nyquist plots of (a) Ni_3Mn/CC, (b) Ni_3Co/CC, (c) Ni/CC, (d) CC and (e) RuO_2 electrodes at various potentials.

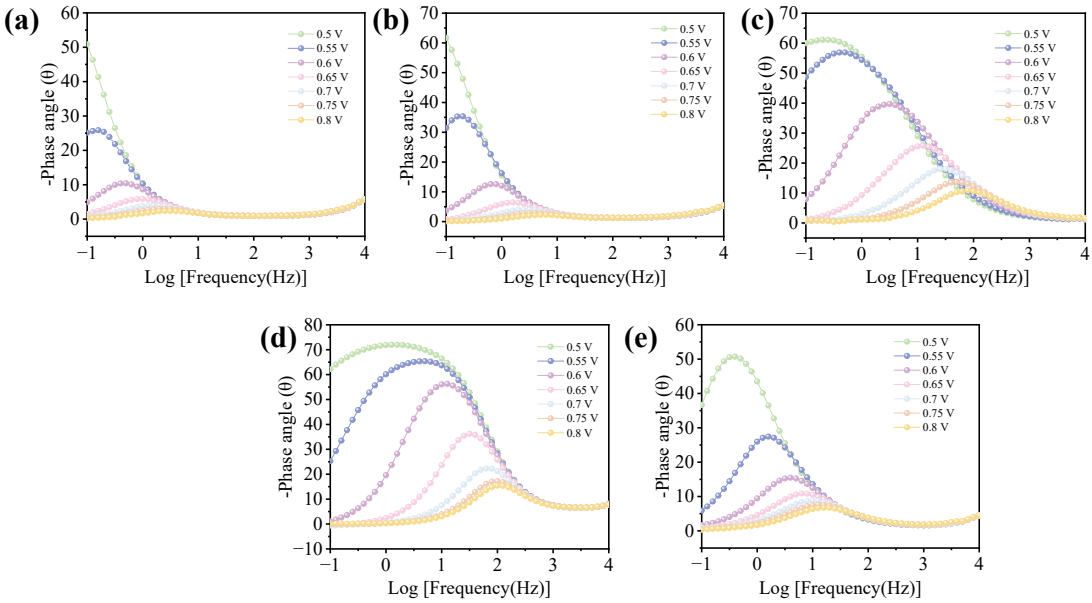

Fig S11. Bode phase angle plots of (a) Ni_3Mn/CC, (b) Ni_3Co/CC, (c) Ni/CC, (d) CC and (e) RuO_2 electrodes at various potentials.

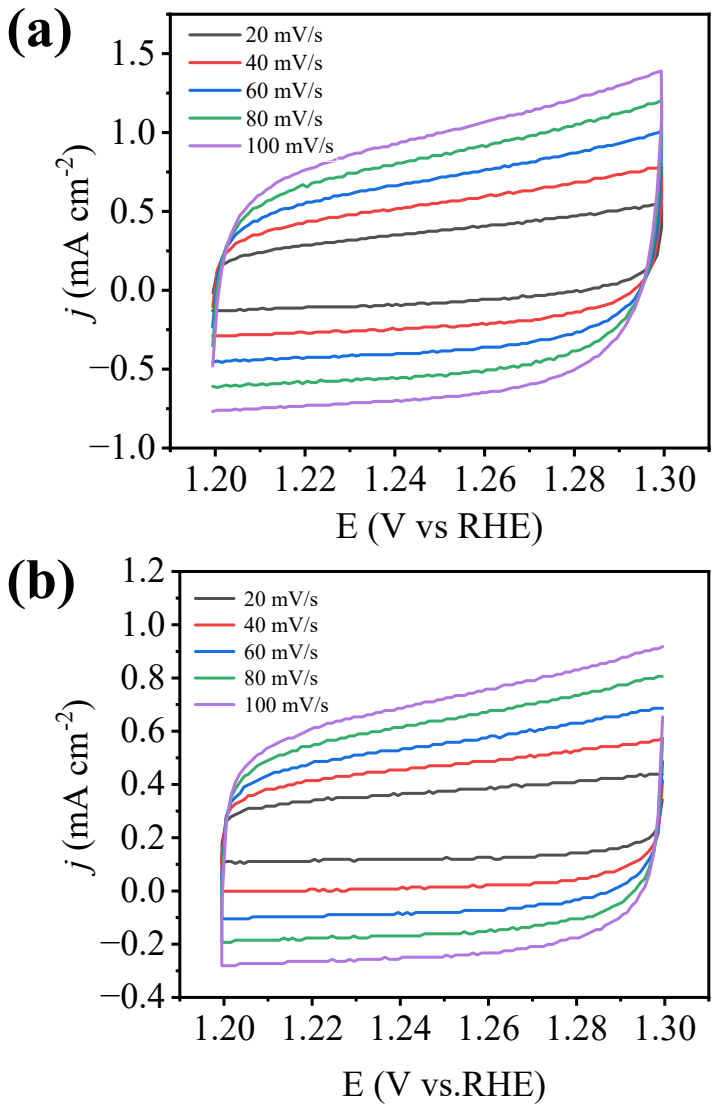

Fig S12. CV curves of Ni_3Fe/CC samples at different scan rates from 20 to 100mV s^{-1} in (a) 1 M KOH and (b) 1 M KOH + 0.5 M NaCl electrolytes.

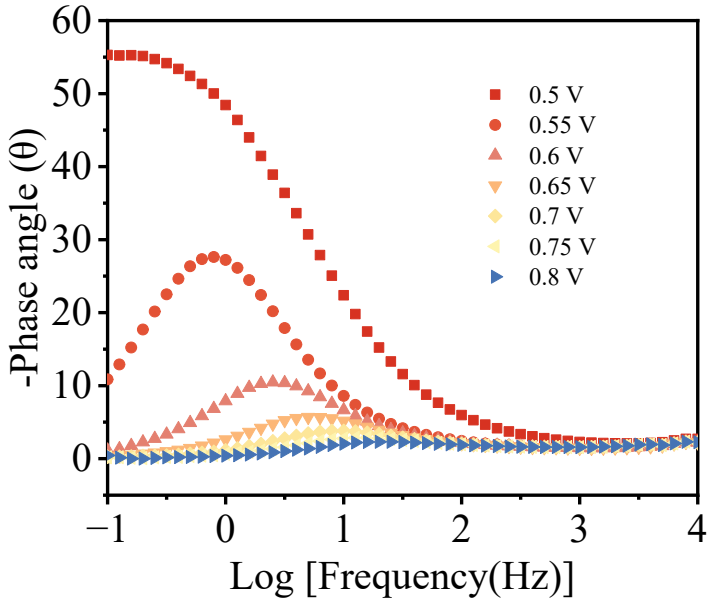

Fig S13. Bode phase angle plots of Ni_3Fe/CC sample in 1 M KOH + 0.5 M NaCl electrolytes.

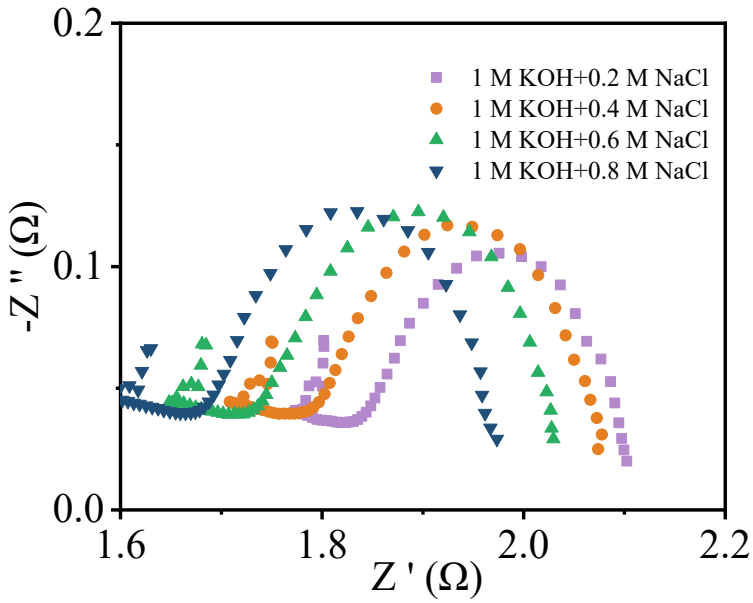

Fig S14. EIS of Ni_3Fe/CC sample in different Cl^- concentrations (0.2, 0.4, 0.6, 0.8 M).

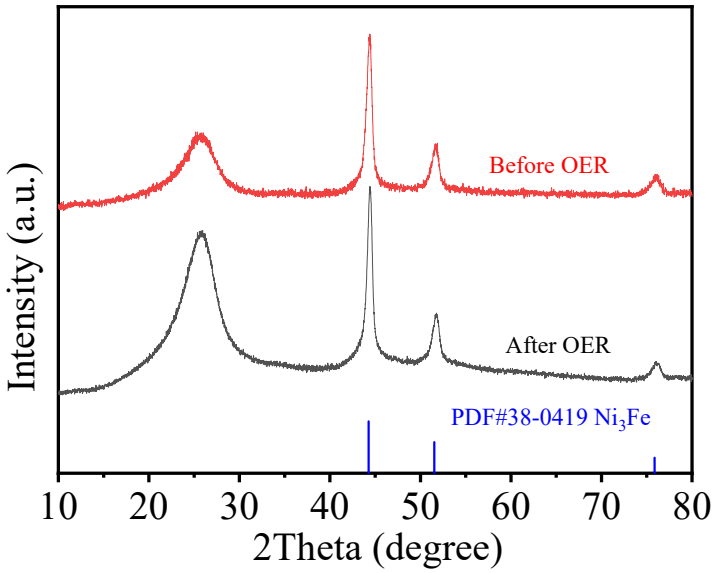

Fig S15. XRD patterns of the Ni_3Fe/CC before and after 500 h stability test.

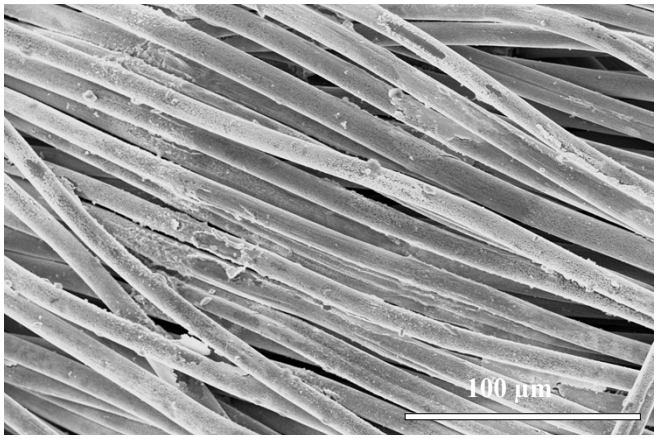

Fig S16. SEM image of Ni_3Fe/CC after 500 h stability test.

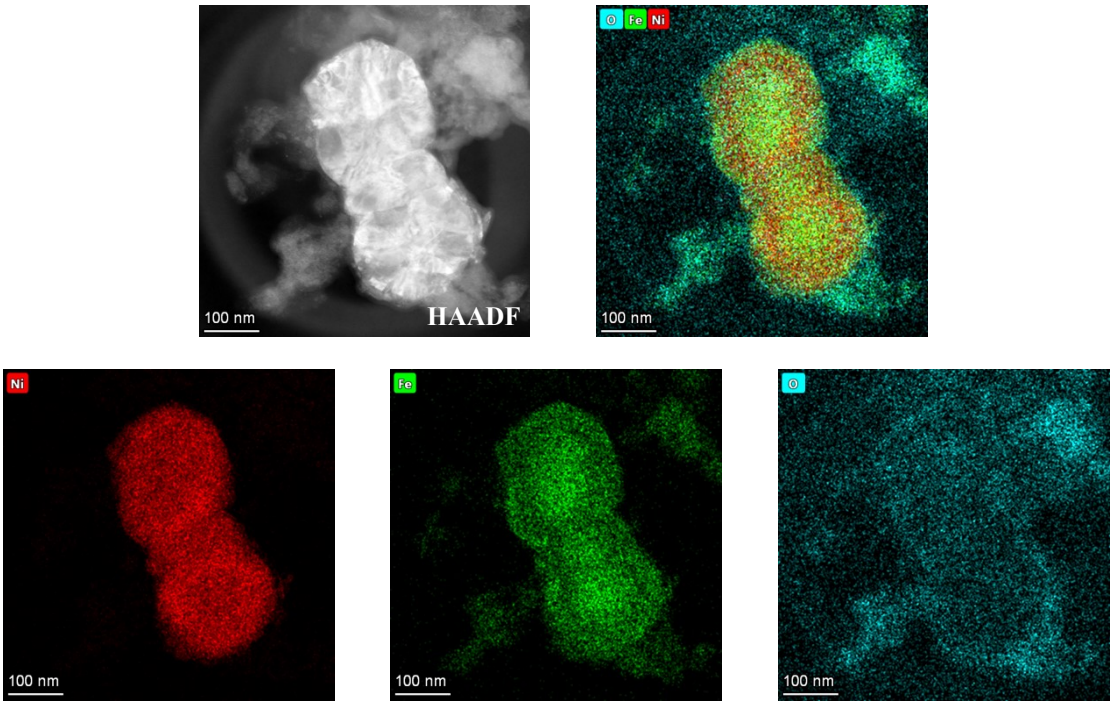

Fig S17. HR-TEM images and elemental mapping images of Ni, Fe and O in Ni_3Fe/CC after OER.

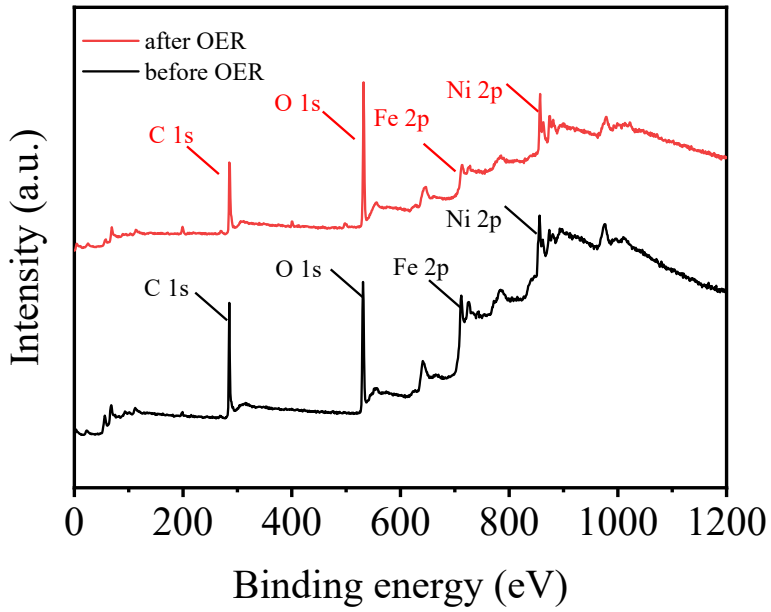

Fig S18. The XPS spectra of Ni_3Fe/CC before and after OER.

3. Supplementary Table

Table S1. Comparison of the OER performance of Ni_3Fe/CC catalyst with other reported OER catalysts

Catalyst	Electrolyte	Substrate	Current density (mA cm^{-2})	Overpotential (mV)	Ref
Ni-MOF/NF-Fe	1 M KOH	NF	100	246	1
NiO	1 M KOH	G P	10	316	2
Gd, Fe-NiO	1 M KOH	GCE	10	227	3
NiS	1 M KOH	GCE	10	320	4
Cr–FeNi LDH	1 M KOH	ESS	10	280	5
α/β-$NiMoO_4$	1 M KOH	NF	10	270	6
a-Ru+NiMoOx	1 M KOH	GC	10	220	7
r_{GO}/Ni_2P	1 M KOH	GCE	10	283	8
$Ni_{32}Fe$	1 M KOH	GCE	10	291	9
$NiFeCoCrW_{0.2}$	1 M KOH	SSWE	10	220	10
$NiO/NiFe_2O_4$	1 M KOH	GCE	10	302	11
Ce-$NiCo_2O_4$	1 M KOH	GCE	10	270	12
Ni_3N/NF	1 M KOH	NF	10	316	13
NiFeOOH	1 M KOH	GCE	10	347	14
Vo-α-Fe_2O_3@AuNSs	1 M KOH	GCE	10	282	15
FeCoNiMnCu	1 M KOH	CNTs	10	293	16
Fe-NiS_2@$NaBH_4$	1 M KOH	NF	10	233	17
FeP	1 M KOH	GPC	10	278	18
NiFeS-2	1 M KOH	GF	10	290	19
$NiFe/W_{0.3}C$	1 M KOH	NC	10	290	20
Ni_3Fe/CC	1 M KOH	CC	10	234	This work

4.References

1. L. Feng, W. Chen, B. Ma, W. Xie, Y. Xia, Z. Zhou, J. Su, R. Zhong and R. Zou, Advanced Functional Materials, 2026, 36, e18095.
2. L. Bruno, M. Scuderi, F. Priolo and S. Mirabella, Sustainable Energy & Fuels, 2022, 6, 4498-4505.
3. Y. Wang, Y. Liu, S. Liu, Y. Qin, J. Liu, X. Jia, Q. Jiang, X. Wang, Y. Zhao, L. Liu, H. Liu, H. Zhao, Y. Jiang, D. Liang, H. Wu, B. Jia, X. Qu, H. Li and M. Qin, Advanced Functional Materials, 2025, 35, 2500118.
4. P. Luo, H. Zhang, L. Liu, Y. Zhang, J. Deng, C. Xu, N. Hu and Y. Wang, ACS Applied Materials & Interfaces, 2017, 9, 2500-2508.
5. Y. Lv, X. Deng, J. Ding and Y. Zhou, Scientific Reports, 2024, 14, 902.
6. J. Zhu, Q. Zhou, L. Wang, W. Zhou, M. Chen, X. Liu, D. Gao and D. Chao, Advanced Energy Materials, 2024, 14, 2304554.
7. J. Li, Y. Zhu, C. Li, Q. Zhang, J. Rong, S. Guo, N. Alonso-Vante, L. Yang, M.-H. Yeh, W.-H. Huang, X. Yu, H. Cheng and J. Ma, Nature Communications, 2025, 16, 8827.
8. P. Li, R. Chen, S. Tian and Y. Xiong, ACS Sustainable Chemistry & Engineering, 2019, 7, 9566-9573.
9. M. Yu, G. Moon, E. Bill and H. Tüysüz, ACS Applied Energy Materials, 2019, 2, 1199-1209.
10. T. Zhang, H.-F. Zhao, Z.-J. Chen, Q. Yang, N. Gao, L. Li, N. Luo, J. Zheng, S.-D. Bao, J. Peng, X. Peng, X.-W. Liu and H.-B. Yu, Nature Communications, 2025, 16, 3327.
11. G. Liu, X. Gao, K. Wang, D. He and J. Li, International Journal of Hydrogen Energy, 2016, 41, 17976-17986.
12. X. Wang, J. Hu, T. Lu, H. Wang, D. Sun, Y. Tang, H. Li and G. Fu, Angewandte Chemie International Edition, 2025, 64, e202415306.
13. M. S. Metaxa, I. Vamvasakis and G. S. Armatas, Small, 2026, 22, e13136.
14. Z. Wang, S. Han, Y. Zhang and Y. Wang, Fuel, 2024, 357, 129946.
15. H. Zhang, P. Li, H. Zhou, J. Xu, Q. Jiang, J. H. L. Hadden, Y. Wang, M. Wang, S. Chen, F. Xie and D. J. Riley, Nano Energy, 2022, 94, 106968.
16. P. Guo, D. Liu, H. Yang, P. Chen, M. Zhang, X. Ding, C. Zheng, H. Pan and R. Wu, ACS Nano, 2026, 20, 4152-4165.
17. G. Xiong, H. Deng, Y. Chen, Q. Wu, X. Zhou and W. Yao, ACS Catalysis, 2025, 15, 13948-13957.
18. J. Masud, S. Umapathi, N. Ashokaan and M. Nath, Journal of Materials Chemistry A, 2016, 4, 9750-9754.
19. B.-Q. Li, S.-Y. Zhang, C. Tang, X. Cui and Q. Zhang, Small, 2017, 13, 1700610.
20. E. Jang, J. Cho, J. Kim and J. Kim, Applied Surface Science, 2024, 663, 160201.